

Enabling Validation for Robust Few-Shot Recognition

Hanxin Wang^{1,*} Tian Liu^{2,*} Shu Kong^{1,3}

¹University of Macau ²Texas A&M University ³Institute of Collaborative Innovation

website: <https://hannawang09.github.io/projects/vest/>

Abstract

*Few-Shot Recognition (FSR) tackles classification tasks by training with minimal task-specific labeled data. Prevailing methods adapt or finetune a pretrained Vision-Language Model (VLM) and augment the scarce training data by retrieving task-relevant but noisy samples from open data sources. The finetuned VLM generalizes decently well to the task-specific in-distribution (ID) test data but struggles with out-of-distribution (OOD) test data. This motivates our study of robust FSR with VLM finetuning. The core challenge of FSR is data scarcity, extending beyond limited training data to a complete lack of validation data. We identify a key paradox as a potential solution: repurposing the retrieved open data for validation. As such retrieved data are inherently OOD compared with the task-specific ID training data, finetuned VLMs yield degraded performance on the retrieved data. This causes the validation logic to favor the pretrained model without any finetuning, hindering improvements w.r.t generalization. To resolve this dilemma, we introduce a novel validation strategy that harmonizes performance gain and degradation on the few-shot ID data and the retrieved data, respectively. Our validation enables parameter selection for partial finetuning and checkpoint selection, mitigating overfitting and improving test-data generalization. We unify this strategy with robust learning into a cohesive framework: **Validation-Enabled Stage-wise Tuning (VEST)**. Extensive experiments on the established ImageNet OOD benchmarks show that VEST significantly outperforms existing VLM adaptation methods, achieving state-of-the-art FSR performance on both ID and OOD data.*

1. Introduction

Few-Shot Recognition (FSR) frames the scenario when a classification task provides a small amount of labeled training data for object categories of interest. The recent FSR literature exploits pretrained Vision-Language Models (VLMs) [32, 48] through various adaptation methods (Fig. 2). In real applications, the adapted VLM inevitably encounters

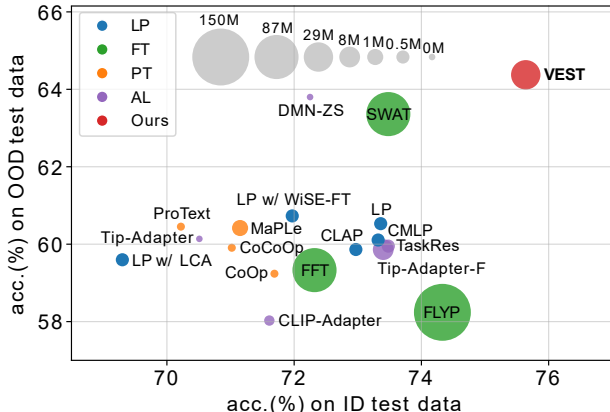


Figure 1. **Summary of benchmarking results of VLM adaptation methods** w.r.t accuracies on the ID and OOD test data. We also mark the number of learned parameters of each method. All the compared methods work on a pretrained CLIP ViT-B/16 VLM [48] under the 16-shot setting; refer to Sec. 4 for dataset details, Fig. 2 for the compared methods, and Table 1 for detailed results. Our method VEST (Sec. 3.4) significantly outperforms the compared methods with a moderate number of learned parameters.

out-of-distribution (OOD) test data that have distribution shifts compared with the task-specific in-distribution (ID) data. This challenges the generalization of the adapted VLM, motivating our work on *robust FSR* with VLM finetuning.

Status Quo. Current FSR methods commonly leverage pretrained VLMs, adapting them via parameter-efficient finetuning (PEFT) such as prompt tuning (PT) [4, 25, 26, 50, 71], or linear probing (LP) [33, 53, 54], or lightweight adapter learning (AL) [9, 68]. The recent work [35] motivates FSR from a data annotation perspective, prioritizing accuracy over parameter efficient finetuning. It shows that finetuning the VLM’s visual encoder on the few-shot training data outperforms PEFT methods. It also recommends leveraging external open data sources, e.g., the VLM’s pretraining data, to augment the few-shot training examples. Moreover, while early FSR methods tune and report results on the test set, the current literature is converging on a more realistic setting that realizes the data scarcity issue and eschews a validation set [33, 35, 54]. Nevertheless, a crucial aspect remains unaddressed: the robustness of FSR methods to OOD test data, which have distribution shifts compared with the training

*The first two authors make equal contributions.

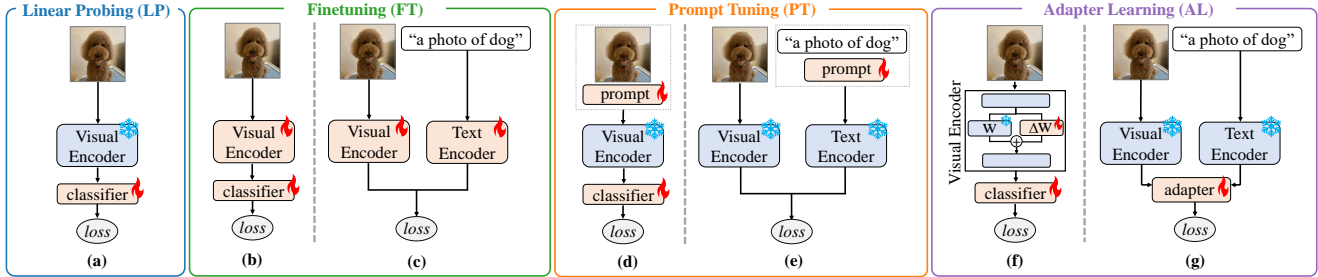


Figure 2. **Diagrams of prevailing VLM adaptation methods.** We categorize them into four groups: **Linear Probing (LP)** learns a linear classifier on top of a pretrained visual encoder [48] (a). **Finetuning (FT)** methods learn to update the VLM via a cross entropy loss [35] (b) or a contrastive loss [11] (c). **Prompt Tuning (PT)** methods learn visual prompts [22] (d) or text prompts [71] (e) in the input space by freezing the VLM. **Adapter Learning (AL)** methods freeze the VLM and learn lightweight modules, such as low-rank matrices [19, 64] (f) or some layers of parameters [68] (g).

data though they capture the same object categories. We rigorously study robust FSR under the realistic setting and address the issue of a complete lack of validation data.

Insights. The core challenge of FSR is data scarcity, extending beyond limited training data to a complete lack of validation data. The recent FSR work [35] retrieves task-relevant though noisy samples from external data sources to augment the few-shot training data. It defaults hyperparameters (e.g., epochs and learning rate) to what are widely used in the literature. Yet, no prior works have exploited the retrieved data for validation. The retrieved samples are inherently OOD compared with the task-specific ID training data. Consequently, finetuned VLM yields degraded performance on the retrieved samples. Hence, directly using them as the validation data for checkpoint selection will choose the original VLM without any finetuning, hindering improvements w.r.t generalization to both ID and OOD test data (Fig. 4). We address this dilemma with a novel validation strategy, which harmonizes the performance gain and degradation on the ID training data and the retrieved data (Fig. 5). Our validation enables selecting a checkpoint that generalizes well to ID and OOD test data. Importantly, it also allows tuning hyperparameters such as parameters of the VLM to finetune towards better generalization (Fig. 6). We incorporate the validation strategy with robust learning techniques [37] over both the few-shot ID data and the retrieved data, deriving a simple yet effective finetuning pipeline (Fig. 7): **Validation-Enabled Stage-wise Tuning (VEST)**. Extensive experiments demonstrate that VEST significantly outperforms various VLM adaptation methods (Fig. 1).

Contributions. We make three key contributions:

1. We establish the robust FSR problem and comprehensively evaluate existing VLM-based FSR methods.
2. We propose a novel validation strategy by exploiting the few-shot ID training data and external data source, allowing hyperparameter tuning and checkpoint selection for better generalization to both ID and OOD test data.
3. We present a robust finetuning pipeline with our valida-

tion strategy, significantly outperforming existing VLM-based FSR methods w.r.t both ID and OOD accuracy.

2. Related work

Few-Shot Recognition (FSR). Modern approaches exploit a pretrained VLM, but most of them freeze the VLM and only learn prompt tokens [25, 50, 62, 70, 71] or lightweight adapters [9, 55, 68, 69]. Some investigate finetuning the VLM [11, 28, 35], but [28] shows that finetuning can destroy pretrained features and degrade the generalization ability. [60] mitigates this issue by ensembling the finetuned and the pretrained models. However, no prior work has comprehensively benchmarked VLM adaptation methods w.r.t OOD generalization, measuring accuracies on both ID and OOD test data. Thus, improving the OOD generalization of adapted VLM with limited ID training data remains an open question. Moreover, not until recently have FSR methods turned hyperparameters on a held-out labeled validation set or even the test set [33, 35, 54]. Such an artificial practice leads to significant data leakage and produces over-optimistic results and unfair comparisons. In this work, we adopt a realistic setup that eschews a validation set for hyperparameter tuning [35, 54] and conduct the first comprehensive study of existing VLM adaptation methods w.r.t robust FSR.

Open Data. There exists abundant publicly available data, not only facilitating training more generalizable and robust models [15, 27] but also enabling VLM pretraining [6, 21, 48, 61]. From the open data sources, recent works retrieve task-relevant data to boost performance in zero-shot recognition [20, 31, 34, 44, 57], complex reasoning [13, 30], and image generation [3, 5]. The recent FSR method [35] also retrieves relevant open data to augment the few-shot training data, but it has not evaluated the model’s performance on OOD test data nor exploited such data for validation. Our work explores using such data for validation, a crucial component that has been underexplored (until now!) in FSR, which has severe data scarcity issue. Our developed validation strategy allows hyperparameter tuning and check-



Figure 3. Example images of two classes from the ID training set (marked by black border), the OOD test sets (marked by blue border), and the retrieved images from the open data source LAION-400M [52] (marked by orange border). Visually, the retrieved examples are not only OOD compared with the ID images, but also noisy due to linguistic ambiguity. For example, `lemon` also means a pale yellow color, hence an image of a lemon/yellow umbrella is retrieved (ref. the top-right visual).

point selection, significantly boosts the generalization and robustness of finetuned VLM for FSR.

Robustness and Generalization can mean different aspects depending on the context, but both aim to address real-world scenarios where training and test data are drawn from different distributions [17, 51]. For example, some works focus on adversarial robustness, aiming to train models that are robust to adversarial attacks [7, 10, 29, 37, 51]. Some others study the generalization ability to novel classes by evaluating how a model performs in downstream tasks, which adapt the model to the downstream novel classes [25, 26, 70]. Another line of research investigates the generalization and robustness of models to test data with distribution shift, i.e., those that deviate from the training distribution but still belong to the same classes of training data [17, 28, 53, 60]. Our work belongs to the last literature. In this context, prior works have introduced dedicated OOD test sets [2, 14, 49, 58] and developed methods to predict OOD performance based on metrics on the ID data [1, 23, 39, 53]; prevailing methods turn to data augmentation [16, 41, 45, 66], sophisticated finetuning techniques [11, 28], and ensembling [59, 60]. Differently, our work not only comprehensively studies the generalization and robustness of FSR methods that adapt VLMs, but also develops novel approaches, including a validation strategy and robust learning with adversarial perturbed data and real-world open data (explained below).

3. Validation-Enabled Few-Shot Finetuning

We first formulate the problem of robust FSR. We then introduce a novel validation strategy, allowing checkpoint selection and layer selection. Lastly, we present our final method.

3.1. Problem Formulation

Training and Validation Protocol. In a realistic scenario, we have a downstream task to solve and an open-source VLM and open data for leverage [35]. The downstream task is defined as K -way classification. It provides only a small set of labeled data, denoted as $\mathcal{D} = \{(\mathbf{I}_i, y_i)\}_{i=1}^n$, where \mathbf{I}_i and $y_i \in \{1, \dots, K\}$ are the i^{th} image and its label,

respectively. Each class has m labeled examples, i.e., the so-called “ m -shot” setting and $n = m * K$. The VLM consists of a visual encoder $V(\cdot)$ and a text encoder $T(\cdot)$. We denote the image and text embedding features as $\mathbf{x}_i = V(\mathbf{I}_i)$ and $\mathbf{t}_i = T(y_i)$, respectively. FSR methods can adapt the VLM to the task-specific data in \mathcal{D} . They can also exploit the open data to facilitate few-shot learning. Importantly, there does not exist a validation set of task-specific data [35, 54].

Evaluation Protocol. We evaluate FSR methods on ID and OOD test sets. The ID test images follow the same distribution of the task-specific training data (i.e., both are sampled from the same dataset). The OOD test images have distribution shifts but still capture the same classes as the training data. Fig. 3 displays some ID and OOD images.

Baseline. To derive our techniques, we start by finetuning the visual encoder using the cross-entropy (CE) loss \mathcal{L}_{CE} over the few-shot training data:

$$\mathcal{L}_{CE} = \frac{1}{|\mathcal{D}|} \sum_{(\mathbf{I}_i, y_i) \in \mathcal{D}} \ell_{CE}(\mathbf{I}_i, y_i) \quad (1)$$

where $\ell_{CE}(\mathbf{I}, y) = -\log \frac{\exp(\mathbf{w}_y^T \cdot V(\mathbf{I}))}{\sum_{j=1}^K \exp(\mathbf{w}_j^T \cdot V(\mathbf{I}))}$, and \mathbf{w}_j is the classifier weight for class- j initialized as the corresponding text embedding feature. Quantitative results present in this section are on the datasets and model detailed in Sec. 4.

3.2. Enabling Validation for Checkpoint Selection

In machine learning, validation is crucial for checkpoint selection to avoid overfitting [47]. Due to data scarcity, FSR cannot provide a validation set and is especially prone to overfitting [35, 54], hurting the generalization ability of trained models (Fig. 4-right). Yet, the unavailability of a validation set does not mean no validation methods. Inspired by the recent work [35], which retrieves task-relevant data from open data resources to augment few-shot training images, we exploit such data for validation. As our work does not focus on RA approaches, we adopt the one proposed in [35, 44] (details in Sec. C of the supplement).

A straightforward idea is to pack the retrieved data as the validation set. However, the retrieved data is OOD compared

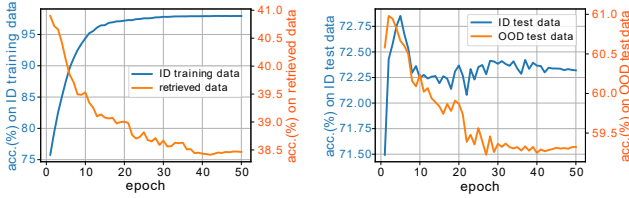


Figure 4. **Left:** Finetuning on the ID training data certainly improves the accuracy on them but yields degraded performance on the retrieved data, which deviates from the training distribution (ref. Fig. 3). This shows that the retrieved data cannot serve as a validation set. **Right:** Finetuned models quickly suffer from overfitting, degrading dramatically after epoch-8 on both ID and OOD test sets. This shows an urgent need of validation for checkpoint selection.

to the task-specific few-shot training data, as illustrated in Fig. 3. Consequently, the finetuned model on the ID data yields degraded performance on the retrieved data (Fig. 4-left). Hence, solely relying on the accuracy on the retrieved data will select the original non-finetuned VLM, preventing effective finetuning to improve the generalization ability.

We present a validation strategy based on “performance gains” on the ID training data and the retrieved data. Specifically, for each checkpoint, say at epoch- i , we calculate its training accuracy (acc_{ID}^i) and the accuracy on the retrieved data (acc_{RT}^i). We place all the checkpoints on a 2D plane with x and y specifying the two accuracies (Fig. 5-left). Then, for the t^{th} checkpoint, we compute its “performance gain” on the ID training data as $\Delta_{ID}^t = \text{acc}_{ID}^t - \min_i(\text{acc}_{ID}^i)$, and on the retrieved data as $\Delta_{RT}^t = \text{acc}_{RT}^t - \min_i(\text{acc}_{RT}^i)$. We measure the generalization ability of this checkpoint using their harmonic mean (in spirit of F1 score), dubbed **gF1** and illustrated in Fig. 5-left:

$$\text{gF1}^t = 2 \times \frac{\Delta_{ID}^t \times \Delta_{RT}^t}{\Delta_{ID}^t + \Delta_{RT}^t}. \quad (2)$$

For the example in Fig. 5-left, we select the checkpoint at epoch-3, which has the largest gF1. We verify this selection by comparing these checkpoints w.r.t accuracies on the OOD and ID test data in Fig. 5-right. Results show that the selected checkpoint does generalize robustly well to the test data.

3.3. Enabling Validation for Layer Selection

Among various hyperparameters to tune, an underexplored one is to determine what parameters to finetune. Intuitively, learning too few parameters may insufficiently adapt the pretrained model to the downstream task, while learning too many parameters may easily overfit to the few-shot training data, distort pretrained features and degrade generalization [28]. Moreover, low-level layers of pretrained parameters are more general, while high-level ones are more tailor to downstream tasks. Hence, we extend our validation strategy to determine k for **partially finetuning (PFT)** the top- k layers or blocks in a Transformer.

Per the practice of validation, we vary k and finetune the top- k layers of the visual encoder $V(\cdot)$. For each k , we plot a

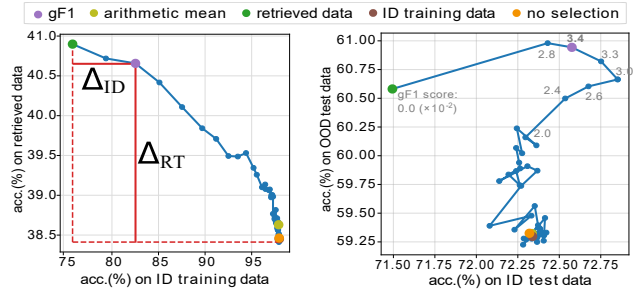


Figure 5. **Left:** Our validation strategy selects the checkpoint at epoch-3 that maximizes the gF1 score (Eq. 2). **Right:** We compare checkpoints selected by different methods: our gF1 score, the arithmetic mean of accuracies on the ID training data and retrieved data, the accuracy on the retrieved data only, the accuracy on the ID training data only, and no selection (i.e., using the last checkpoint). Clearly, gF1 selects a checkpoint that performs robustly well and generalizes to both ID and OOD test data.

curve for the checkpoints w.r.t accuracies on the ID training data and the retrieved data (Fig. 6A). Across k , the curves do not have common start and end points to fairly compare their gF1 scores (Fig. 6B). We address this issue by first selecting the checkpoint for each k (Fig. 6C), and then select the final one, just among these selected checkpoints, that has the max gF1 score (Fig. 6D). The final chosen checkpoint reflects the tuned k . To validate the effectiveness of our validation strategy w.r.t layer selection, we compare the accuracies of the selected checkpoints for different k on the ID and OOD test sets. Fig. 6-right lists the results, demonstrating that our validation strategy effectively determines the top- k layers to PFT for better robustness and generalization.

3.4. VEST: Validation-Enabled Stage-wise Tuning

With our validation strategy, we present our final method by adopting two well-known techniques: Retrieval-based Augmentation (RA) and Adversarial Perturbation (AP).

Retrieval-based Augmentation (RA) is a modern technique that leverages open data source to solve a downstream task [34, 35, 44, 57]. It retrieves examples relevant to the K classes concerned by the downstream task, and uses them to augment training data. We adopt such data for partially finetuning the VLM. Let’s denote the set of retrieved data as $\mathcal{D}_R = \{(\mathbf{I}_i, y_i)\}_{i=1}^N$. We compute the CE loss over it: $\mathcal{L}_{RA} = \frac{1}{|\mathcal{D}_R|} \sum_{(\mathbf{I}_i, y_i) \in \mathcal{D}_R} \ell_{CE}(\mathbf{I}_i, y_i)$.

Adversarial Perturbation (AP) can be embedded into learning to train adversarially robust models [37]. AP perturbs input example by purposefully maximizing the training loss, e.g., through the projected gradient descent (PGD) to perturb the example with the negative CE loss ℓ_{CE} [10]. While AP typically applies to input data \mathbf{I} , we apply it to the features \mathbf{x} with PFT for better efficiency (Fig. 7-right). Denote this process as $\hat{\mathbf{x}} = \text{AP}(\mathbf{x}, y; T, \epsilon)$, which recursively perturbs the feature \mathbf{x} (from class- y) for T times. The t^{th} iteration outputs $\mathbf{x}^t = \mathbf{x}^{t-1} + \alpha \cdot \text{sign}(\nabla_{\mathbf{x}} \ell_{CE}(\mathbf{x}^{t-1}, y))$,

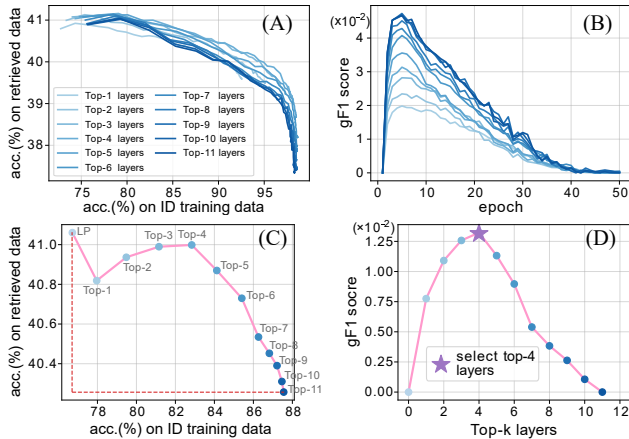


Figure 6. **Layer selection via the proposed validation strategy.** (A) With a specific k , we partially finetune (PFT) the top- k layers / blocks of the visual encoder and plot the accuracies of checkpoints on the ID training data and retrieved data. (B) For each checkpoint, we calculate its gF1 score. Apparently, these scores are not comparable across k due to their inconsistent start and end points in (A). (C) We address this issue by first selecting the checkpoint based on gF1 for each PFT of top- k layers, and then plotting them w.r.t accuracies on the ID training data and retrieved data to recompute a gF1 score for each. (D) Such a plot allows fair comparison of gF1 scores of these checkpoints and helps select the top-4 layers to finetune. **Right:** We list the detailed results on ID and OOD test sets, showing that the selected checkpoint by PFT the top-4 layers indeed performs robustly well, remarkably outperforming linear probing and full finetuning.

finetuned layers	ID test		OOD test			
	IN	avg.	IN-V2	IN-S	IN-A	IN-R
zero-shot linear probing	66.75	57.15	60.91	46.16	47.53	73.99
	71.52	60.65	64.48	49.10	50.79	78.21
top-1	72.30	61.17	65.44	49.36	51.29	78.57
top-2	72.89	61.70	66.07	49.81	51.91	79.01
top-3	73.19	61.78	66.15	49.95	51.96	79.06
top-4	<u>73.35</u>	61.80	<u>66.23</u>	<u>49.89</u>	52.04	<u>79.02</u>
top-5	73.41	61.74	66.46	49.79	51.95	78.78
top-6	73.40	61.61	66.49	49.60	51.79	78.55
top-7	73.20	61.28	66.22	49.35	51.41	78.14
top-8	73.03	61.02	65.98	49.21	51.16	77.74
top-9	72.99	60.90	65.95	49.14	50.91	77.58
top-10	72.89	60.91	65.90	49.11	50.97	77.68
top-11	72.83	60.92	65.87	49.02	51.19	77.59
FFT [35]	72.32	59.33	64.85	48.10	49.03	75.33

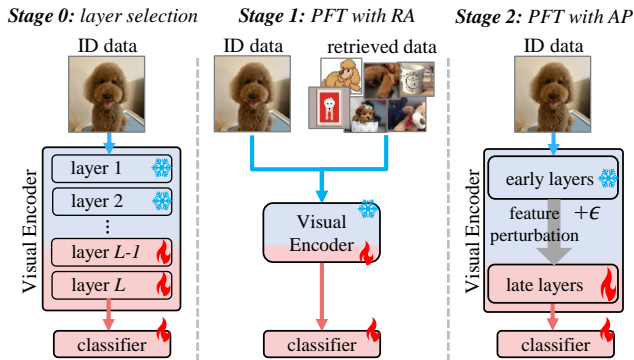


Figure 7. **Flowchart of the proposed VEST.** First, it runs our validation strategy to select top layers to partially finetune (PFT) the visual encoder. Then, it exploits retrieved task-relevant, though noisy, examples from the VLM’s pretraining dataset to augment the few-shot ID training data, and partially finetunes the selected layers. Lastly, it adversarially perturbs features (Eq. 3) to robustly finetune these layers over only the few-shot ID training data.

where $\mathbf{x}^0 = \mathbf{x}$, and α controls the perturbation intensity. This is followed by clamping with ϵ , which constrains the perturbed data to be within a bounded neighborhood $[-\epsilon, \epsilon]$ of the original data. To contrast the typical CE loss in Eq. 1, we use a separate loss notation to indicate the use of AP:

$$\mathcal{L}_{AP} = \frac{1}{|\mathcal{D}|} \sum_{(\mathbf{x}_i, y_i) \in \mathcal{D}} \ell_{CE}(\text{AP}(\mathbf{x}_i, y_i; T, \epsilon), y_i) \quad (3)$$

One-Stage training. With RA and AP, one may jointly minimize the losses to partially finetune the visual encoder:

$$\mathcal{L} = \mathcal{L}_{CE} + \mathcal{L}_{AP} + \mathcal{L}_{RA}. \quad (4)$$

Notably, the retrieved examples have label noises, distributional shifts compared with task-specific training images (Fig. 3), and imbalanced class distributions [35, 44]. Conse-

quently, this one-stage finetuning does not yield remarkable improvements (Table 2). Hence, we propose the stage-wise finetuning pipeline, presented next.

Stage-wise training is shown to mitigate issues caused by data imbalance [24] and domain gaps [35], and serves as a transfer learning paradigm [38]. We develop VEST that incorporates RA and AP to PFT the visual encoder in three stages (Fig. 7): (1) layer selection for PFT with validation, (2) PFT with both ID few-shot training data and the retrieved data, and (3) PFT with AP on the ID few-shot training data. Compared with one-stage training, VEST not only achieves better results w.r.t accuracies on ID and OOD test data, but also significantly reduces training cost (Table 2).

4. Experiments

Through experiments, we validate the effectiveness of our validation strategy, analyze the stages in our VEST, and demonstrate its state-of-the-art performance. We first describe the datasets and VLMs for experiments, introduce the compared methods, and present important details of implementation. We then carry out in-depth analyses of our methods and benchmark their results.

Datasets, Model, and Protocol. We follow [53] to adopt the ImageNet-based large-scale OOD benchmarking protocol. Specifically, based on ImageNet (IN) [8], it randomly samples few-shot training data of its 1,000 classes as the ID training data, and uses its official validation set as the ID test set. Moreover, it uses four OOD variants of ImageNet as the OOD test sets, including ImageNet-V2 (IN-V2) [49], ImageNet-Sketch (IN-S) [58], ImageNet-Adversarial (IN-A) [18], and ImageNet-Rendition (IN-R) [17]. The four OOD datasets capture different distribution shifts, such

Table 1. **Benchmarking results of different VLM adaptation methods** on the ID test set ImageNet (IN) and the OOD test sets ImageNet-V2 (IN-V2), ImageNet-Sketch (IN-S), ImageNet-A (IN-A), and ImageNet-Rendation (IN-R). We report the top-1 accuracy on the IN and OOD benchmarks. For convenient comparison, for each method, we report averaged accuracy (marked in blue) across four OOD test sets. We categorize existing adaptation methods into four groups (Fig. 2): prompt tuning, adapter learning, linear probing, and finetuning. We list zero-shot methods as references. We run all the methods with their original validation protocols over the CLIP ViT-B/16 model [48], under 16-, 8-, and 4-shot settings. Particularly, if a method originally uses a validation set of ID data for tuning, we do the same here, reporting over-optimistic results for it and marking its validation method as “ID test acc”. Note that both SWAT and VEST adopt RA, using the same set of retrieved data to augment the training data. Yet, owing to our validation strategy that enables layer selection and checkpoint selection, VEST resoundingly outperforms SWAT by +2.16 and +1.02 accuracy gains on ID and OOD test data.

	method	venue&year	validation	16-shot						8-shot		4-shot	
				ID		OOD				ID	OOD	ID	OOD
				IN	avg.	IN-V2	IN-S	IN-A	IN-R	IN	avg.	IN	avg.
Zero-Shot	Prompting [48]	ICML’21	–	66.75	57.15	60.91	46.16	47.53	73.99	66.75	57.15	66.75	57.15
	CuPL [46]	ICCV’23	–	69.64	60.04	63.37	49.03	50.68	77.07	69.64	60.04	69.64	60.04
Prompt Tuning	CoOp [71]	IJCV’22	ID test acc.	71.69	59.24	64.34	47.20	50.20	75.21	70.80	59.68	70.29	59.74
	CoCoOp* [70]	CVPR’22	ID test acc.	71.02	59.91	64.07	48.75	50.63	76.18	–	–	–	–
	MaPLe [25]	CVPR’23	ID test acc.	71.15	60.42	64.49	48.69	50.91	77.58	70.76	60.23	70.58	60.13
	VPT _{shallow} [22]	ECCV’22	ID test acc.	72.75	60.80	65.70	49.33	49.68	78.56	71.48	60.29	70.31	59.76
	VPT _{deep} [22]	ECCV’22	ID test acc.	72.78	59.12	65.04	47.83	47.11	76.49	71.22	59.30	70.54	59.71
	ProText* [26]	AAAI’25	ID test acc.	70.22	60.45	63.54	49.45	51.47	77.35	–	–	–	–
Adapter Learning	Tip-Adapter [68]	ECCV’22	ID test acc.	70.51	60.14	63.23	48.64	50.88	77.80	70.07	60.05	69.70	60.05
	Tip-Adapter-F [68]	ECCV’22	ID test acc.	73.40	59.85	65.43	47.95	49.08	76.95	71.77	59.91	70.74	59.84
	CLIP-Adapter [9]	IJCV’23	ID test acc.	71.61	58.03	64.05	46.66	47.87	73.53	70.25	57.74	69.55	58.36
	TaskRes [63]	CVPR’23	ID test acc.	73.48	59.95	65.10	48.12	49.96	76.62	71.91	60.04	71.28	59.51
	DMN-ZS* [69]	CVPR’24	ID test acc.	72.25	63.80	65.17	53.20	58.28	78.55	–	–	–	–
	LoRA [19]	ICLR’22	ID test acc.	72.89	60.63	65.31	48.40	50.67	78.12	71.82	60.36	70.62	59.88
Linear Probing	LP [48]	ICML’21	ID test acc.	73.36	60.53	65.33	48.91	49.76	78.12	72.45	59.77	71.44	59.55
	LP w/ WiSE-FT [60]	CVPR’22	ID test acc.	71.97	60.73	64.47	49.43	50.69	78.33	71.37	60.48	70.82	60.20
	CMLP [33]	CVPR’23	ID test acc.	73.32	60.11	64.88	48.41	49.58	77.56	72.21	59.93	70.90	59.56
	LP w/ LCA [53]	ICML’24	ID test acc.	69.30	59.60	62.41	48.52	49.65	77.81	69.23	59.48	69.15	59.61
	CLAP [54]	CVPR’24	val-free	72.97	59.86	65.11	48.00	49.53	76.81	71.56	59.53	70.91	59.17
Finetuning	FLYP [11]	CVPR’23	ID test acc.	74.33	58.24	65.50	47.28	45.75	74.43	72.52	58.78	71.80	59.17
	FFT [35]	CVPR’25	val-free	72.32	59.33	64.85	48.10	49.03	75.33	71.18	59.33	70.35	59.21
	SWAT [35]	CVPR’25	val-free	73.48	63.35	66.51	54.86	50.86	81.20	72.47	63.15	72.03	63.02
	VEST	ours	gF1 score	75.64	64.37	68.58	54.79	52.96	81.17	74.56	64.22	73.41	63.56

*These results are copied from the original papers.

as variations in data collection, sketches, adversarial images, and artistic renditions. ImageNet is released for non-commercial research and educational purposes, and the OOD datasets are open-source under the MIT License. Refer to Fig. 3 for some visual examples and supplementary Sec. B for more details. Following the literature [33, 54, 56, 70, 71], we use the CLIP ViT-B/16 model as the pretrained VLM, on which there is no concern about overlap or data leakage between its pretraining data and the above ImageNet-related datasets [48]. Moreover, we use LAION-400M [52] as the external data resource, which is open-source under CC-BY 4.0 License and has weak affinity to ImageNet [6]. From LAION-400M, we follow [35] to retrieve task-relevant data for the 1,000 classes of ImageNet. For each class, we retrieve ~ 500 images to augment the few-shot labeled data, and another ~ 50 images to construct our validation set. We conduct experiments under 4-, 8-, and 16-shot settings, and the ablation study in the 16-shot setting.

Compared Methods. We compare representative VLM adaptation methods categorized into four groups: prompt tuning [22, 25, 26, 46, 70, 71], adapter learning [9, 19, 63,

64, 68, 69], linear probing [33, 48, 53, 54, 60], and finetuning [11, 35, 60]. Fig. 2 depicts their diagrams. For fair comparison, we run their open-source code to train on the same ID training data. Most of these methods rely on a validation set or even the test set for hyperparameter tuning and checkpoint selection, as also reported by [35, 54]. For them, we use the ID test set for tuning. Arguably, this helps them report over-optimistic results. Moreover, CLAP [54], few-shot finetuning (FFT) and SWAT [35] are validation-free methods, we adopt their reported hyperparameters and train them without validation. Moreover, other than our VEST, SWAT also leverages external data to facilitate FST. In experiments, we use the same retrieved data for them. We provide more details in supplementary Sec. F.

Implementation Details. We implement all the methods with PyTorch and train on a single NVIDIA RTX 4090 GPU (24GB), except CoOp and MaPLe, on which we run on A40 GPU (48GB) due to their demands on large GPU memories. For all the methods, we apply data augmentation: random resize, random crop, and horizontal flip. In training, we use the AdamW optimizer and a cosine-annealing learning rate

Table 2. **Stage-wise finetuning strategies.** The left table compares the results of incorporating RA and AP with PFT and FFT (for reference), along with wall-clock time for 10 epochs of finetuning. PFT finetunes the top-4 blocks of VLM visual encoder, determined by our validation strategy. For all the models, we apply this strategy to select checkpoints. Either RA or AP can improve ID or OOD accuracy, with RA yielding notable OOD accuracy gains. Yet, combining them does not improve further even at a substantially increased computation cost. Hence, we perform PFT with RA in the first stage. The right table compares the results of finetuning different stage-1 models by different stage-2 methods. Applying AP in stage-2 significantly boosts ID performance and improves OOD accuracy further. We suggest the best pipeline, i.e., VEST (highlighted in blue), is to adopt RA for PFT in the first stage and continue to PFT with AP in the second stage. VEST achieves the best ID and OOD accuracy with remarkable efficiency.

Stage-1		accuracy		wall-clock time (h)	
tuning	RA	AP	ID test set		OOD test sets
FFT	✓		72.58	60.94	0.5
		✓	72.89 ^{+0.31}	63.28 ^{+2.34}	6.4
		✓	72.75 ^{+0.17}	59.58 ^{-1.36}	2.2
	✓	✓	72.70 ^{+0.12}	61.90 ^{+0.96}	59.2
PFT			73.35	61.80	0.4
	✓		73.56 ^{+0.21}	63.60 ^{+1.80}	3.5
		✓	73.63 ^{+0.28}	61.86 ^{+0.06}	1.0
	✓	✓	73.55 ^{+0.20}	63.39 ^{+1.59}	20.1

Stage-1		Stage-2		accuracy		wall-clock time (h)
tuning	RA	tuning	AP	ID test set	OOD test sets	
				73.56	63.60	3.5
PFT w/		FFT		75.38 ^{+1.82}	64.07 ^{+0.47}	3.5 + 0.5
RA		PFT		75.39 ^{+1.83}	64.24 ^{+0.64}	3.5 + 0.4
		PFT	✓	75.64^{+2.08}	64.37^{+0.77}	3.5 + 1.0
				73.55	63.39	20.1
PFT w/		FFT		75.48 ^{+1.93}	63.79 ^{+0.40}	20.1 + 0.5
RA+AP		PFT		75.51 ^{+1.96}	64.06 ^{+0.67}	20.1 + 0.4
		PFT	✓	75.61 ^{+2.06}	64.03 ^{+0.64}	20.1 + 1.0

scheduler. For our method, we set the learning rates to $1e-6$ for the backbone and $1e-3$ for the classifier, and batch size to 64. We finetune the VLM for 10 epochs per stage and use our validation strategy for checkpoint selection (Fig. 5). For AP, we set the max iteration $T = 10$ and magnitude $\epsilon = 0.007$; we analyze the impacts of ϵ in Fig. 8. We perform AP on both the task-specific and retrieved data.

4.1. Experimental Results

Benchmarking results. Table 1 compares our VEST against a multitude of VLM adaptation methods. Notably, for the methods that assume a validation set of ID data for hyper-parameter tuning and checkpoint selection, we do the same here, reporting their over-optimistic accuracies and marking their validation method as “ID test acc.” Moreover, a few methods are validation-free, including CLAP, FFT, and SWAT. Both SWAT and our VEST adopt RA, exploiting the same set of retrieved data in our work. Yet, owing to our validation strategy, which enables layer selection and checkpoint selection, our VEST resoundingly outperforms SWAT. Next, we present in-depth analyses and ablation study.

Validation-enabled layer selection. We first remind the reader that our validation strategy allows layer selection for partial finetuning (PFT), which resoundingly outperforms the validation-free few-shot finetuning (FFT) method [35] and linear probing. Fig. 6 in Sec. 3.3 has reported the results. Hereafter in experiments, PFT refers to finetuning the top-4 blocks of VLM’s visual encoder.

Stage-wise finetuning with RA and AP. We analyze the benefit of stage-wise finetuning and the use of RA and AP. Table 2 lists detailed results. With RA and AP, PFT still outperforms FFT, corroborating that our validation strategy helps determine what parameters to finetune to achieve more robust finetuned models. Moreover, while applying either RA and AP improves ID and OOD accuracy for PFT, jointly

Table 3. **Cross-dataset validation.** With each one of the four OOD datasets as the validation set, we apply our validation strategy for checkpoint selection in few-shot finetuning (FFT [35]). We report the accuracies of the selected checkpoint on the ID test set, the other three OOD test sets, as well as the val-set itself. For reference, the first row lists the results of FFT without validation. Regardless of the OOD dataset used for validation, our validation strategy can select a checkpoint that resoundingly outperforms the validation-free FFT method (ref. accuracy gains in subscripts).

val-set	ID test		OOD test		
	IN	IN-V2	IN-S	IN-A	IN-R
w/o val [35]	72.32	64.85	48.10	49.03	75.33
IN-V2	72.75 ^{+0.43}	65.54	49.02 ^{+0.92}	51.04 ^{+2.01}	77.69 ^{+2.36}
IN-S	72.58 ^{+0.26}	65.54 ^{+0.69}	49.39	50.72 ^{+1.69}	78.12 ^{+2.79}
IN-A	72.68 ^{+0.36}	65.46 ^{+0.61}	48.72 ^{+0.62}	51.15	77.09 ^{+1.76}
IN-R	72.58 ^{+0.26}	65.54 ^{+0.69}	49.39 ^{+1.29}	50.72 ^{+1.69}	78.12

applying them does not improve further, even with significantly increased computation cost. In contrast, by adopting another stage to continue finetuning, we obtain remarkable accuracy gains on both ID and OOD test data. In this study, we derive our final method VEST, which first carry out PFT with RA, then continue PFT with AP. VEST also has decent computation efficiency.

Cross-dataset validation. To further validate our validation strategy, we simulate a distributionally-shifted validation set by using each one of the four OOD test sets. We perform validation for checkpoint selection through few-shot finetuning (FFT) [35]. Table 3 reports the results, showing that, regardless of the OOD dataset used for validation, our validation strategy can select a checkpoint that resoundingly outperforms the recent validation-free FFT method [35].

Validation for tuning the perturbation magnitude ϵ . Fig. 8 shows a trade-off between ID and OOD test accuracies by varying ϵ . It also validates the effectiveness of the proposed gF1 score for tuning ϵ . The gF1 helps set ϵ , which

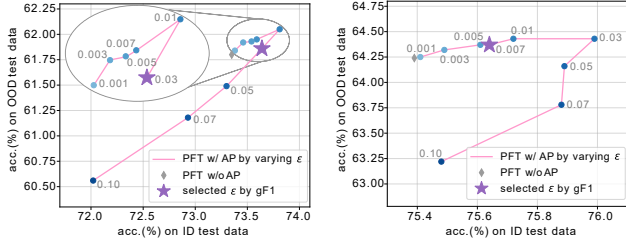


Figure 8. **Impacts of the perturbation magnitude ϵ on the ID and OOD test accuracies.** We apply AP to partially finetune the pretrained visual encoder of CLIP (left) and the finetuned visual encoder after stage-1 of VEST (right), respectively. With a specific ϵ , we use the proposed gF1 score to select a checkpoint and report its accuracy on the ID and OOD test data. For comparison, we mark the performance of a vanilla PFT that does not apply AP. Clearly, applying AP improves ID and OOD accuracies over the vanilla PFT. We set ϵ to $7e-3$ in VEST throughout this work.

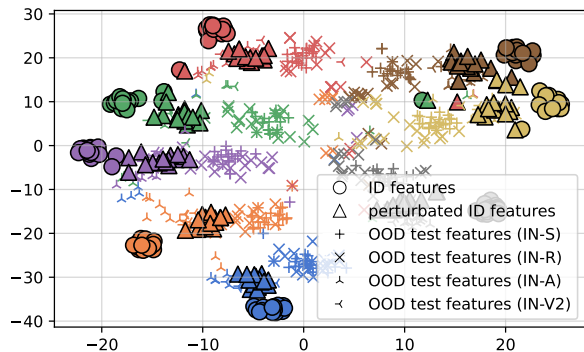


Figure 9. **t-SNE visualization** of features of ID training data, their adversarially perturbed (AP) features, and features of OOD test data from eight random classes. Clearly, OOD test features are greatly shifted from the ID training features, demonstrating the challenge of OOD generalization. AP features are also shifted from the ID training features due to the AP mechanism, but they are close to ID features, owing to ϵ in Eq. 3 which controls the distance of AP features to the ID features. Interestingly, the AP features are located between the OOD test features and the ID features. Intuitively, such AP features serve as a bridge, explaining why adopting AP improves robust finetuning and OOD generalization.

leads to a finetuned model that achieves a good balance of ID and OOD accuracies.

Visualization of features. Fig. 9 visualizes the features of ID training data, their adversarially perturbed features, and features of OOD test data. It intuitively demonstrates how AP features bridges the ID training features and OOD test features and explains why adopting AP in VLM finetuning improves OOD generalization.

Validation for finetuning DINOv2. Tab. 4 shows that our gF1 score generalizes to the DINOv2 visual foundation model [42], allowing checkpoint selection and layer selection, leading to higher ID and OOD accuracies than the recent FSL method [35]. See Sec. E.2 for more details.

Table 4. Our gF1 score enhances the few-shot finetuning (FFT) [35] of the DINOv2 visual foundation model. Here, we run FFT to finetune DINOv2 for 150 epochs in the 16-shot setting. During this course, we use gF1 to select a checkpoint, which outperforms the FFT’s default checkpoint, i.e., the last one determined by its validation-free configuration. Moreover, gF1 allows layer selection for partial finetuning (PFT), which yields further improvements. Lastly, our VEST performs the best.

methods	validation	ID test		OOD test			
		IN	avg.	IN-V2	IN-S	IN-A	IN-R
FFT	val-free	77.01	55.56	68.25	47.88	48.44	57.66
FFT	gF1 score	77.73	58.50	69.60	50.26	53.20	60.92
PFT	gF1 score	77.15	60.62	69.44	52.85	52.76	67.44
VEST	gF1 score	79.29	67.60	72.54	60.04	59.04	78.77

5. Impacts and Limitations

Impacts. Robust FSR via VLM adaptation has broad impacts on real-world applications such as data annotation [35], clinical diagnosis [40] and autonomous driving [36, 43], where the adapted models must reliably generalize to test data that have distribution shifts. Our work advances the research on this topic. However, methods that can improve OOD generalization could also lead to over-generalization, i.e., the adapted model could fail to alert when encountering open-set [27], anomalous [12], counterfactual [67], or adversarial [65] test data. This is a potential negative impact.

Limitations and Future Work. We note certain limitations that warrant a discussion. First, RA may not work well in highly specialized tasks whose data are hard to obtain from open data resources. Studying these tasks requires future work to develop new benchmarks. Second, while the AP method proves effective, the perturbed examples lack diversity. Intuitively, diversifying adversarial perturbations could improve OOD generalization further, suggesting future work for controllable adversarial perturbation. Third, although our validation strategy is general, we have not used it to tune other hyperparameters, such as the learning rate and weight decay, nor have we applied it to other FSR methods. This remains a valuable direction for future work.

6. Conclusions

We study robust few-shot recognition (FSR) and investigate VLM adaptation methods w.r.t test accuracy on both in-distribution (ID) and out-of-distribution (OOD) data. The core challenge in FSR is data scarcity, not only limited training data but also a complete lack of validation data. Hence, we first propose a novel and effective validation method by jointly considering the training accuracy and the accuracy on data retrieved from open data sources. We further leverage such open data to finetune VLM in a stage-wise manner with robust learning. Extensive analyses lead to our final method VEST, which significantly outperforms existing VLM adaptation methods on the ImageNet OOD benchmarks.

Acknowledgments

This work is supported by CK Foundation and Plato Initiative, Science and Technology Development Fund of Macau SAR (0067/2024/ITP2), University of Macau (SRG2023-00044-FST), and the Institute of Collaborative Innovation.

References

- [1] Christina Baek, Yiding Jiang, Aditi Raghunathan, and J Zico Kolter. Agreement-on-the-line: Predicting the performance of neural networks under distribution shift. In *Advances in Neural Information Processing Systems (NeurIPS)*, 2022. 3
- [2] Andrei Barbu, David Mayo, Julian Alverio, William Luo, Christopher Wang, Dan Gutfreund, Josh Tenenbaum, and Boris Katz. Objectnet: A large-scale bias-controlled dataset for pushing the limits of object recognition models. In *Advances in Neural Information Processing Systems (NeurIPS)*, 2019. 3
- [3] Andreas Blattmann, Robin Rombach, Kaan Oktay, Jonas Müller, and Björn Ommer. Retrieval-augmented diffusion models. In *Advances in Neural Information Processing Systems (NeurIPS)*, 2022. 2
- [4] Guangyi Chen, Weiran Yao, Xiangchen Song, Xinyue Li, Yongming Rao, and Kun Zhang. Plot: Prompt learning with optimal transport for vision-language models. In *International Conference on Learning Representations (ICLR)*, 2023. 1
- [5] Wenhui Chen, Hexiang Hu, Chitwan Saharia, and William W Cohen. Re-imagen: Retrieval-augmented text-to-image generator. In *International Conference on Learning Representations (ICLR)*, 2023. 2
- [6] Mehdi Cherti, Romain Beaumont, Ross Wightman, Mitchell Wortsman, Gabriel Ilharco, Cade Gordon, Christoph Schuhmann, Ludwig Schmidt, and Jenia Jitsev. Reproducible scaling laws for contrastive language-image learning. In *IEEE/CVF Conference on Computer Vision and Pattern Recognition (CVPR)*, 2023. 2, 6, 12
- [7] Francesco Croce and Matthias Hein. Reliable evaluation of adversarial robustness with an ensemble of diverse parameter-free attacks. In *International Conference on Machine Learning (ICML)*, 2020. 3
- [8] Jia Deng, Wei Dong, Richard Socher, Li-Jia Li, Kai Li, and Li Fei-Fei. Imagenet: A large-scale hierarchical image database. In *IEEE/CVF Conference on Computer Vision and Pattern Recognition (CVPR)*, 2009. 3, 5, 12
- [9] Peng Gao, Shijie Geng, Renrui Zhang, Teli Ma, Rongyao Fang, Yongfeng Zhang, Hongsheng Li, and Yu Qiao. Clip-adapter: Better vision-language models with feature adapters. *International Journal of Computer Vision (IJCV)*, 132(2): 581–595, 2023. 1, 2, 6, 15
- [10] Ian J Goodfellow, Jonathon Shlens, and Christian Szegedy. Explaining and harnessing adversarial examples. *arXiv preprint arXiv:1412.6572*, 2014. 3, 4
- [11] Sachin Goyal, Ananya Kumar, Sankalp Garg, Zico Kolter, and Aditi Raghunathan. Finetune like you pretrain: Improved finetuning of zero-shot vision models. In *IEEE/CVF Conference on Computer Vision and Pattern Recognition (CVPR)*, 2023. 2, 3, 6, 15
- [12] Zhaopeng Gu, Bingke Zhu, Guibo Zhu, Yingying Chen, Ming Tang, and Jinqiao Wang. Anomalygpt: Detecting industrial anomalies using large vision-language models. In *AAAI conference on artificial intelligence (AAAI)*, 2024. 8
- [13] Kelvin Guu, Kenton Lee, Zora Tung, Panupong Pasupat, and Mingwei Chang. Retrieval augmented language model pre-training. In *International Conference on Machine Learning (ICML)*, 2020. 2
- [14] Dan Hendrycks and Thomas Dietterich. Benchmarking neural network robustness to common corruptions and perturbations. In *International Conference on Learning Representations (ICLR)*, 2019. 3
- [15] Dan Hendrycks, Mantas Mazeika, and Thomas Dietterich. Deep anomaly detection with outlier exposure. In *International Conference on Learning Representations (ICLR)*, 2019. 2
- [16] Dan Hendrycks, Norman Mu, Ekin D Cubuk, Barret Zoph, Justin Gilmer, and Balaji Lakshminarayanan. Augmix: A simple data processing method to improve robustness and uncertainty. In *International conference on machine learning (ICLR)*, 2020. 3
- [17] Dan Hendrycks, Steven Basart, Norman Mu, Saurav Kadavath, Frank Wang, Evan Dorundo, Rahul Desai, Tyler Zhu, Samyak Parajuli, Mike Guo, et al. The many faces of robustness: A critical analysis of out-of-distribution generalization. In *IEEE/CVF International Conference on Computer Vision (ICCV)*, 2021. 3, 5, 12
- [18] Dan Hendrycks, Kevin Zhao, Steven Basart, Jacob Steinhardt, and Dawn Song. Natural adversarial examples. In *IEEE/CVF Conference on Computer Vision and Pattern Recognition (CVPR)*, 2021. 3, 5, 12
- [19] Edward J Hu, yelong shen, Phillip Wallis, Zeyuan Allen-Zhu, Yuanzhi Li, Shean Wang, Lu Wang, and Weizhu Chen. LoRA: Low-rank adaptation of large language models. In *International Conference on Learning Representations (ICLR)*, 2022. 2, 6, 15
- [20] Ahmet Iscen, Mathilde Caron, Alireza Fathi, and Cordelia Schmid. Retrieval-enhanced contrastive vision-text models. In *International Conference on Learning Representations (ICLR)*, 2024. 2
- [21] Chao Jia, Yinfei Yang, Ye Xia, Yi-Ting Chen, Zarana Parekh, Hieu Pham, Quoc Le, Yun-Hsuan Sung, Zhen Li, and Tom Duerig. Scaling up visual and vision-language representation learning with noisy text supervision. In *International Conference on Machine Learning (ICML)*, 2021. 2
- [22] Menglin Jia, Luming Tang, Bor-Chun Chen, Claire Cardie, Serge Belongie, Bharath Hariharan, and Ser-Nam Lim. Visual prompt tuning. In *European Conference on Computer Vision (ECCV)*, 2022. 2, 6, 15
- [23] Yiding Jiang, Vaishnavh Nagarajan, Christina Baek, and J Zico Kolter. Assessing generalization of SGD via disagreement. In *International Conference on Learning Representations (ICLR)*, 2022. 3
- [24] Bingyi Kang, Saining Xie, Marcus Rohrbach, Zhicheng Yan, Albert Gordo, Jiashi Feng, and Yannis Kalantidis. Decoupling representation and classifier for long-tailed recognition. *arXiv preprint arXiv:1910.09217*, 2019. 5

- [25] Muhammad Uzair Khattak, Hanoona Rasheed, Muhammad Maaz, Salman Khan, and Fahad Shahbaz Khan. Maple: Multi-modal prompt learning. In *IEEE/CVF Conference on Computer Vision and Pattern Recognition (CVPR)*, 2023. 1, 2, 3, 6, 15
- [26] Muhammad Uzair khattak, Muhammad Ferjad, Naseer Muz-zamal, Luc Van Gool, and Federico Tombari. Learning to prompt with text only supervision for vision-language models. In *AAAI Conference on Artificial Intelligence (AAAI)*, 2025. 1, 3, 6, 15
- [27] Shu Kong and Deva Ramanan. Opengan: Open-set recognition via open data generation. In *IEEE/CVF International Conference on Computer Vision (ICCV)*, 2021. 2, 8
- [28] Ananya Kumar, Aditi Raghunathan, Robbie Matthew Jones, Tengyu Ma, and Percy Liang. Fine-tuning can distort pre-trained features and underperform out-of-distribution. In *International Conference on Learning Representations (ICLR)*, 2022. 2, 3, 4, 12
- [29] Alexey Kurakin, Ian J Goodfellow, and Samy Bengio. Adversarial examples in the physical world. In *Artificial intelligence safety and security*, pages 99–112. Chapman and Hall/CRC, 2018. 3
- [30] Patrick Lewis, Ethan Perez, Aleksandra Piktus, Fabio Petroni, Vladimir Karpukhin, Naman Goyal, Heinrich Küttler, Mike Lewis, Wen-tau Yih, Tim Rocktäschel, Sebastian Riedel, and Douwe Kiela. Retrieval-augmented generation for knowledge-intensive nlp tasks. In *Advances in Neural Information Processing Systems (NeurIPS)*, 2020. 2
- [31] Alexander Cong Li, Ellis Langham Brown, Alexei A Efros, and Deepak Pathak. Internet explorer: Targeted representation learning on the open web. In *International Conference on Machine Learning (ICML)*, 2023. 2
- [32] Junnan Li, Ramprasaath Selvaraju, Akhilesh Gotmare, Shafiq Joty, Caiming Xiong, and Steven Chu Hong Hoi. Align before fuse: Vision and language representation learning with momentum distillation. In *Advances in Neural Information Processing Systems (NeurIPS)*, 2021. 1
- [33] Zhiqiu Lin, Samuel Yu, Zhiyi Kuang, Deepak Pathak, and Deva Ramanan. Multimodality helps unimodality: Cross-modal few-shot learning with multimodal models. In *IEEE/CVF Conference on Computer Vision and Pattern Recognition (CVPR)*, 2023. 1, 2, 6, 12, 13, 15
- [34] Haotian Liu, Kilho Son, Jianwei Yang, Ce Liu, Jianfeng Gao, Yong Jae Lee, and Chunyuan Li. Learning customized visual models with retrieval-augmented knowledge. In *IEEE/CVF Conference on Computer Vision and Pattern Recognition (CVPR)*, 2023. 2, 4, 12
- [35] Tian Liu, Huixin Zhang, Shubham Parashar, and Shu Kong. Few-shot recognition via stage-wise retrieval-augmented fine-tuning. In *IEEE/CVF Conference on Computer Vision and Pattern Recognition (CVPR)*, 2025. 1, 2, 3, 4, 5, 6, 7, 8, 12, 13, 14, 15
- [36] Anish Madan, Neehar Peri, Shu Kong, and Deva Ramanan. Revisiting few-shot object detection with vision-language models. In *Advances in Neural Information Processing Systems (NeurIPS)*, 2024. 8
- [37] Aleksander Madry, Aleksandar Makelov, Ludwig Schmidt, Dimitris Tsipras, and Adrian Vladu. Towards deep learning models resistant to adversarial attacks. *arXiv preprint arXiv:1706.06083*, 2017. 2, 3, 4
- [38] Dhruv Mahajan, Ross Girshick, Vignesh Ramanathan, Kaiming He, Manohar Paluri, Yixuan Li, Ashwin Bharambe, and Laurens Van Der Maaten. Exploring the limits of weakly supervised pretraining. In *European Conference on Computer Vision (ECCV)*, 2018. 5
- [39] John P Miller, Rohan Taori, Aditi Raghunathan, Shiori Sagawa, Pang Wei Koh, Vaishaal Shankar, Percy Liang, Yair Carmon, and Ludwig Schmidt. Accuracy on the line: on the strong correlation between out-of-distribution and in-distribution generalization. In *International Conference on Machine Learning (ICML)*, 2021. 3
- [40] Jong Hak Moon, Hyungyung Lee, Woncheol Shin, Young-Hak Kim, and Edward Choi. Multi-modal understanding and generation for medical images and text via vision-language pre-training. *IEEE Journal of Biomedical and Health Informatics*, 26(12):6070–6080, 2022. 8
- [41] Junsoo Oh and Chulhee Yun. Provable benefit of cutout and cutmix for feature learning. In *Advances in Neural Information Processing Systems (NeurIPS)*, 2024. 3
- [42] Maxime Oquab, Timothée Darcet, Théo Moutakanni, Huy V. Vo, Marc Szafraniec, Vasil Khalidov, Pierre Fernandez, Daniel HAZIZA, Francisco Massa, Alaaeldin El-Nouby, Mido Assran, Nicolas Ballas, Wojciech Galuba, Russell Howes, Po-Yao Huang, Shang-Wen Li, Ishan Misra, Michael Rabbat, Vasu Sharma, Gabriel Synnaeve, Hu Xu, Herve Jegou, Julien Mairal, Patrick Labatut, Armand Joulin, and Piotr Bojanowski. DINOv2: Learning robust visual features without supervision. *Transactions on Machine Learning Research*, 2024. 8, 12, 14
- [43] Chenbin Pan, Burhaneddin Yaman, Tommaso Nesti, Abhirup Mallik, Alessandro G Allievi, Senem Velipasalar, and Liu Ren. Vlp: Vision language planning for autonomous driving. In *IEEE/CVF Conference on Computer Vision and Pattern Recognition (CVPR)*, 2024. 8
- [44] Shubham Parashar, Zhiqiu Lin, Tian Liu, Xiangjue Dong, Yanan Li, Deva Ramanan, James Caverlee, and Shu Kong. The neglected tails in vision-language models. In *Proceedings of the IEEE/CVF Conference on Computer Vision and Pattern Recognition (CVPR)*, 2024. 2, 3, 4, 5, 12, 13
- [45] Francesco Pinto, Harry Yang, Ser Nam Lim, Philip Torr, and Puneet Dokania. Using mixup as a regularizer can surprisingly improve accuracy & out-of-distribution robustness. In *Advances in Neural Information Processing Systems (NeurIPS)*, 2022. 3
- [46] Sarah Pratt, Ian Covert, Rosanne Liu, and Ali Farhadi. What does a platypus look like? generating customized prompts for zero-shot image classification. In *IEEE/CVF International Conference on Computer Vision (ICCV)*, 2023. 6
- [47] Lutz Prechelt. Early stopping-but when? In *Neural Networks: Tricks of the trade*, pages 55–69. Springer, 2002. 3
- [48] Alec Radford, Jong Wook Kim, Chris Hallacy, Aditya Ramesh, Gabriel Goh, Sandhini Agarwal, Girish Sastry, Amanda Askell, Pamela Mishkin, Jack Clark, et al. Learning transferable visual models from natural language supervision. In *International Conference on Machine Learning (ICML)*, 2021. 1, 2, 6, 15

- [49] Benjamin Recht, Rebecca Roelofs, Ludwig Schmidt, and Vaishal Shankar. Do imagenet classifiers generalize to imagenet? In *International Conference on Machine Learning (ICML)*, 2019. 3, 5, 12
- [50] Shuwendu Roy and Ali Etemad. Consistency-guided prompt learning for vision-language models. In *International Conference on Learning Representations (ICLR)*, 2024. 1, 2
- [51] Ludwig Schmidt, Shibani Santurkar, Dimitris Tsipras, Kunal Talwar, and Aleksander Madry. Adversarially robust generalization requires more data. In *Advances in Neural Information Processing Systems (NeurIPS)*, 2018. 3
- [52] Christoph Schuhmann, Richard Vencu, Romain Beaumont, Robert Kaczmarczyk, Clayton Mullis, Aarush Katta, Theo Coombes, Jenia Jitsev, and Aran Komatsuzaki. Laion-400m: Open dataset of clip-filtered 400 million image-text pairs. *arXiv preprint arXiv:2111.02114*, 2021. 3, 6, 13
- [53] Jia Shi, Gautam Gare, Jinjin Tian, Siqi Chai, Zhiqiu Lin, Arun Vasudevan, Di Feng, Francesco Ferroni, and Shu Kong. LCA-on-the-line: benchmarking out-of-distribution generalization with class taxonomies. In *International Conference on Machine Learning (ICML)*, 2024. 1, 3, 5, 6, 15
- [54] Julio Silva-Rodriguez, Sina Hajimiri, Ismail Ben Ayed, and Jose Dolz. A closer look at the few-shot adaptation of large vision-language models. In *Proceedings of the IEEE/CVF Conference on Computer Vision and Pattern Recognition (CVPR)*, 2024. 1, 2, 3, 6, 12, 15
- [55] Lin Song, Ruoyi Xue, Hang Wang, Hongbin Sun, Yixiao Ge, Ying Shan, et al. Meta-adapter: An online few-shot learner for vision-language model. In *Advances in Neural Information Processing Systems (NeurIPS)*, 2023. 2
- [56] Junjiao Tian, Zecheng He, Xiaoliang Dai, Chih-Yao Ma, Yen-Cheng Liu, and Zsolt Kira. Trainable projected gradient method for robust fine-tuning. In *IEEE/CVF Conference on Computer Vision and Pattern Recognition (CVPR)*, 2023. 6
- [57] Matthew Wallingford, Vivek Ramanujan, Alex Fang, Aditya Kusupati, Roozbeh Mottaghi, Aniruddha Kembhavi, Ludwig Schmidt, and Ali Farhadi. Neural priming for sample-efficient adaptation. In *Advances in Neural Information Processing Systems (NeurIPS)*, 2023. 2, 4, 12
- [58] Haohan Wang, Songwei Ge, Zachary Lipton, and Eric P Xing. Learning robust global representations by penalizing local predictive power. In *Advances in Neural Information Processing Systems (NeurIPS)*, 2019. 3, 5, 12
- [59] Mitchell Wortsman, Gabriel Ilharco, Samir Ya Gadre, Rebecca Roelofs, Raphael Gontijo-Lopes, Ari S Morcos, Hongseok Namkoong, Ali Farhadi, Yair Carmon, Simon Kornblith, et al. Model soups: averaging weights of multiple fine-tuned models improves accuracy without increasing inference time. In *International Conference on Machine Learning (ICML)*, 2022. 3
- [60] Mitchell Wortsman, Gabriel Ilharco, Jong Wook Kim, Mike Li, Simon Kornblith, Rebecca Roelofs, Raphael Gontijo Lopes, Hannaneh Hajishirzi, Ali Farhadi, Hongseok Namkoong, et al. Robust fine-tuning of zero-shot models. In *IEEE/CVF Conference on Computer Vision and Pattern Recognition (CVPR)*, 2022. 2, 3, 6, 13, 15
- [61] Hu Xu, Saining Xie, Xiaoqing Ellen Tan, Po-Yao Huang, Russell Howes, Vasu Sharma, Shang-Wen Li, Gargi Ghosh, Luke Zettlemoyer, and Christoph Feichtenhofer. Demystifying clip data. In *International Conference on Learning Representations (ICLR)*, 2024. 2
- [62] Hantao Yao, Rui Zhang, and Changsheng Xu. Visual-language prompt tuning with knowledge-guided context optimization. In *IEEE/CVF Conference on Computer Vision and Pattern Recognition (CVPR)*, 2023. 2
- [63] Tao Yu, Zhihe Lu, Xin Jin, Zhibo Chen, and Xinchao Wang. Task residual for tuning vision-language models. In *IEEE/CVF Conference on Computer Vision and Pattern Recognition (CVPR)*, 2023. 6, 15
- [64] Maxime Zanella and Ismail Ben Ayed. Low-rank few-shot adaptation of vision-language models. In *IEEE/CVF Conference on Computer Vision and Pattern Recognition Workshops (CVPRW)*, 2024. 2, 6, 15
- [65] Jiaming Zhang, Qi Yi, and Jitao Sang. Towards adversarial attack on vision-language pre-training models. In *ACM International Conference on Multimedia (ACMMM)*, 2022. 8
- [66] Linjun Zhang, Zhun Deng, Kenji Kawaguchi, Amirata Ghorbani, and James Zou. How does mixup help with robustness and generalization? In *International Conference on Learning Representations (ICLR)*, 2021. 3
- [67] Letian Zhang, Xiaotong Zhai, Zhongkai Zhao, Yongshuo Zong, Xin Wen, and Bingchen Zhao. What if the tv was off? examining counterfactual reasoning abilities of multi-modal language models. In *IEEE/CVF Conference on Computer Vision and Pattern Recognition (CVPR)*, 2024. 8
- [68] Renrui Zhang, Wei Zhang, Rongyao Fang, Peng Gao, Kunchang Li, Jifeng Dai, Yu Qiao, and Hongsheng Li. Tip-adapter: Training-free adaption of clip for few-shot classification. In *European Conference on Computer Vision (ECCV)*, 2022. 1, 2, 6, 15
- [69] Yabin Zhang, Wenjie Zhu, Hui Tang, Zhiyuan Ma, Kaiyang Zhou, and Lei Zhang. Dual memory networks: A versatile adaptation approach for vision-language models. In *IEEE/CVF Conference on Computer Vision and Pattern Recognition (CVPR)*, 2024. 2, 6, 15
- [70] Kaiyang Zhou, Jingkang Yang, Chen Change Loy, and Ziwei Liu. Conditional prompt learning for vision-language models. In *IEEE/CVF Conference on Computer Vision and Pattern Recognition (CVPR)*, 2022. 2, 3, 6, 15
- [71] Kaiyang Zhou, Jingkang Yang, Chen Change Loy, and Ziwei Liu. Learning to prompt for vision-language models. *International Journal of Computer Vision (IJCV)*, 130(9):2337–2348, 2022. 1, 2, 6, 15

Enabling Validation for Robust Few-Shot Recognition

Supplementary Material

This document supplements our main paper with more details. It is organized as follows:

- **Section A** provides code to reproduce our results.
- **Section B** describes datasets used in our experiments and shows more examples of training and testing data.
- **Section C** provides the implementation details of open data retrieval.
- **Section D** presents hyperparameters used in our work.
- **Section E** provides full results of our validation strategy for checkpoint and layer selection with the CLIP and DINOv2 backbone, respectively.
- **Section F** provides more details of the compared methods.

A. Open-Source Code

We include our code as part of the supplementary material, comprising the following key components:

Requirements. Running the code requires Python, PyTorch, and other common packages. We list all dependencies in the *requirements.txt* file for convenient installation. Additionally, we include detailed environment setup instructions in the *README.md* file. Below are the versions of Python and PyTorch used in this work:

- Python: 3.10.16
- PyTorch: 2.0.0

License. We will release our code under the MIT license.

Instructions. We provide detailed instructions for reproducing our experiments in the following markdown files:

- *DATASETS.md* provides detailed steps for installing the datasets used in our experiments, including ImageNet OOD benchmarks, few-shot splits, and retrieval dataset.
- *README.md* provides detailed guidelines on how to set up the environment and run the demo of the proposed methods.

Demo. The code includes three demos to demonstrate the results of our proposed methods in Table 2 and Table 4. In the demonstration, we finetune CLIP ViT-B/16 [6] and DINOv2 ViT-B/14 [42] models for 16-shot learning using ImageNet (IN) as the ID dataset and evaluate the methods both on ImageNet and its four OOD variants, including ImageNet-V2 (IN-V2) [49], ImageNet-Sketch (IN-S) [58], ImageNet-Adversarial (IN-A) [18], and ImageNet-Rendition (IN-R) [17]. The details of the demos are as follows:

- *PFT_demo.ipynb* contains the implementation of *Partial Finetuning* using CLIP model.
- *VEST_demo.ipynb* contains the implementation of *Validation-Enabled Stage-wise Tuning* using CLIP model.
- *VEST_dinov2_demo.ipynb* contains the implementation of *Validation-Enabled Stage-wise Tuning* using DINOv2.

Table 5. **Statistics of datasets for evaluating OOD generalization.** We list the number of classes and images in the test sets for ImageNet and its variants. Following the few-shot OOD evaluation protocol, we randomly sample $\{4, 8, 16\}$ images from the official ImageNet training set to adapt the VLM (referred to as *our training set*) and evaluate the model’s performance on the ImageNet and its variant test sets. Note that in our work, we do not exploit the ImageNet validation set. Instead, we propose a novel validation strategy by exploiting retrieved open data.

dataset	# classes	# test data	dataset description
ImageNet [8] (IN)	1,000	50,000	containing images for 1,000 common classes
ImageNet-V2 [49] (IN-V2)	1,000	10,000	containing OOD images for ImageNet’s 1,000 classes
ImageNet-S [58] (IN-S)	1,000	50,000	containing sketch images for ImageNet’s 1,000 classes
ImageNet-A [18] (IN-A)	200	7,500	containing adversarial images for 200 ImageNet’s classes
ImageNet-R [17] (IN-R)	200	30,000	containing artistic renditions for 200 ImageNet’s classes

B. Benchmarking Datasets

We summarize the datasets used in our experiments in Table 5. Following established protocols from prior work [28, 33, 54], we report the ID test accuracy using ImageNet validation set [8], and OOD test accuracy on the ImageNet variants [17, 18, 49, 58]. For few-shot recognition, we randomly sample $\{4, 8, 16\}$ images from the official ImageNet training set. All methods are evaluated using three independent training runs with different random seeds for data splitting. For the compared methods that rely on a validation set to select checkpoints, we use the official ImageNet validation set, i.e., the ID test set in our experiments, for this purpose. Importantly, our proposed validation strategy does not require any data from the test sets for tuning. Fig. 10 presents additional examples from ImageNet and its variants, illustrating the distribution differences across these datasets.

C. Details of Open Data Retrieval

To find task-relevant data, early methods rely on feature similarities between target class names and pretraining images/texts [34, 57]. But this requires downloading, hosting and computing over hundreds of millions of VLM’s pretraining examples. In contrast, recent works use string matching to find relevant text first and then retrieve corresponding images [35, 44], showing significantly enhanced efficiency and a capability to retrieve more visually diverse images.

Following this line of work [34, 35], we retrieve images



Figure 10. **Comparison of ImageNet training data (as ID), its four variants (as OOD, marked by blue border), and retrieved data from LAION-400M (marked by orange border).** To illustrate the distributional characteristics, we present more examples of the training and testing images by randomly selecting four classes from ImageNet. The visual comparison reveals significant distribution shifts between ID and OOD data. Notably, although the retrieved data enhances sample diversity, it also introduces noisy images due to linguistic ambiguity in the retrieval process.

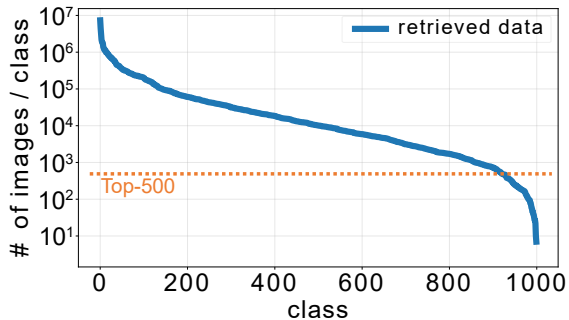


Figure 11. **The retrieved data of ImageNet from LAION-400M [52] follows an imbalanced distribution.** For data retrieval, we use string matching to identify relevant samples, subsequently selecting the 500 most similar images per class by text-to-text feature similarity for training, and randomly sampling 50 images per class from the remaining data for validation.

from LAION-400M [52] via string matching. As illustrated in Fig. 11, the retrieved data for ImageNet follows a long-tail distribution, an imbalanced issue that exists in nature or available pretraining datasets such as LAION-400M and MetaCLIP [44]. For each class, we select 500 images to augment training data. From the remaining data, we randomly sample 50 images per class to form a non-overlapping set used in our validation strategy. It is possible that a class does not have sufficient data or even does not have 500 retrieved

images. In this case, we use all the retrieved images (<500) pertaining to this class for training and do not sample extra data for validation. Additional retrieval examples are provided in Fig. 10.

D. Configuration of Hyperparameter

For our method, we employ the proposed gF1 score for both checkpoint selection and hyperparameter tuning. Following the practice in [33, 35, 44, 60], we initialize the classifier with the average text embedding of 80 OpenAI prompts. The training pipeline includes two standard data augmentations: RandomResizedCrop and RandomHorizontalFlip. We adopt the AdamW optimizer with a cosine annealing learning rate schedule, a batch size of 64, a learning rate of 1e-6 for the backbone, and a learning rate of 1e-3 for the classifier. A warmup phase of 18 iterations is applied, during which the learning rate increases linearly from 1e-8 to its initial value. For partial finetuning (PFT), we train for 50 epochs with a weight decay of 0.1. For VEST, both stage 1 and stage 2 training are conducted for 10 epochs with a weight decay of 0.01. For adversarial perturbation, we perform a grid search of perturbation magnitude ϵ (ref. Eq. (3)) in [0.1, 0.07, 0.05, 0.03, 0.01, 0.007, 0.005, 0.003, 0.001]. The value $\epsilon = 0.007$, chosen by the gF1 score, was used for VEST throughout this work. The impact of ϵ on ID and OOD test accuracy is analyzed in Fig. 8.

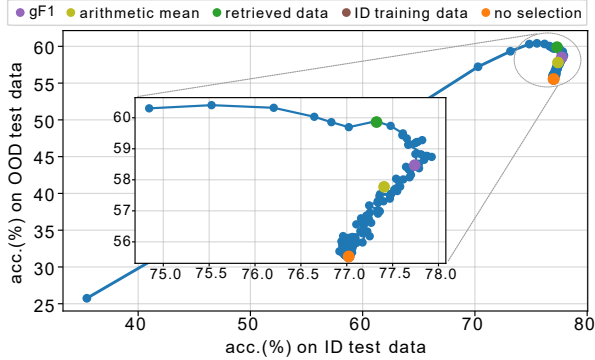


Figure 12. **Checkpoint selection on DINOv2.** We evaluate different validation strategies for checkpoint selection after fully finetuning a DINOv2 ViT-B/14 model for 150 epochs. The right table presents the selected checkpoints (ref. # ckpt) and their detailed performance on ID and OOD test data. The results demonstrate that our gF1 score generalizes effectively to vision foundation models, consistently selecting a checkpoint that achieves robust performance on both ID and OOD test data.

validation methods	# ckpt	ID test		OOD test			
		IN	avg.	IN-V2	IN-S	IN-A	IN-R
no selection	150	77.01	55.56	68.25	47.88	48.44	57.66
ID train data	150	77.01	55.56	68.25	47.88	48.44	57.66
retrieved data	11	77.32	59.89	69.48	51.50	54.12	64.45
arithmetic mean	47	77.40	57.80	69.14	49.82	52.00	60.24
gF1 score	32	77.73	58.50	69.60	50.26	53.20	60.92

Table 6. **Full checkpoint selection results on CLIP.** We fully fine-tune CLIP ViT-B/16 for 50 epochs and compare checkpoint selection based on our proposed gF1 score against several alternatives in Fig. 5-right. This table reports the detailed performance of the checkpoints selected by each method, including the index of the selected checkpoint (ref. # ckpt) and the corresponding ID and OOD test accuracies. The results demonstrate that our gF1 effectively selects a checkpoint that achieves strong performance on both ID and OOD test data.

validation methods	# ckpt	ID test		OOD test			
		IN	avg.	IN-V2	IN-S	IN-A	IN-R
no selection	50	72.32	59.33	64.85	48.10	49.03	75.33
ID train data	44	72.34	59.30	64.83	48.10	48.95	75.32
retrieved data	1	71.49	<u>60.58</u>	64.49	<u>49.10</u>	<u>50.31</u>	78.42
arithmetic mean	35	72.34	59.32	64.82	48.11	49.05	75.31
gF1	3	72.58	60.94	65.54	49.39	50.72	<u>78.12</u>

For the compared methods, we directly adopt their reported hyperparameters and train them on the same few-shot training data for fair comparison. To note, for the methods which require on a validation set, we use the official ImageNet validation set, i.e., the ID test set in our experiments, to help them with checkpoint selection.

E. More about Checkpoint & Layer Selection

E.1. Validation for CLIP

Table 6 details the performance of checkpoints selected by different methods. As expected, selecting based on retrieved-data accuracy alone favors early checkpoints that largely preserve the pretrained VLM due to the OOD nature of the retrieved data. Conversely, selecting by ID training accuracy alone leads to a later, heavily overfitted checkpoint. A naive approach that averages these two accuracies still fails to avoid overfitting. Our proposed validation strategy, however, successfully selects the checkpoint that performs well on both ID and OOD test data.

Table 7. **Layer selection on DINOv2.** We perform partial finetuning (PFT) on the top- k layers of the vision model. A clear trade-off exists between ID and OOD test accuracy across different values of k . Our proposed validation method selects PFT top-1 layers, which provides a good balance between ID and OOD performance and remarkably outperforms linear probing and full finetuning.

finetuned layers	gF1 ($\times 10^{-2}$)	ID test		OOD test			
		IN	avg.	IN-V2	IN-S	IN-A	IN-R
linear probing	0.00	76.72	59.86	68.82	52.45	51.20	66.97
top-1	0.43	77.15	60.62	69.44	52.85	52.76	67.44
top-2	0.33	77.66	<u>60.07</u>	69.58	52.35	53.07	65.29
top-3	0.00	77.80	59.60	69.86	51.72	53.32	63.51
top-4	0.10	77.82	59.42	69.97	51.48	53.49	62.73
top-5	0.08	77.97	59.19	69.85	51.22	53.48	62.22
top-6	0.09	78.01	59.10	69.79	50.96	53.60	62.04
top-7	0.04	78.07	58.97	69.63	50.71	53.83	61.70
top-8	0.00	<u>78.02</u>	58.95	69.70	50.60	53.84	61.66
top-9	0.02	<u>78.02</u>	58.98	69.69	50.66	53.95	61.62
top-10	0.06	78.01	59.12	69.86	50.75	54.11	61.75
top-11	0.07	78.01	59.12	69.85	50.65	54.25	61.73
FFT [35]	-	77.01	55.56	68.25	47.88	48.44	57.66

E.2. Validation for DINOv2

To further evaluate the effectiveness of our validation method, we extend its application to the vision foundation model, specifically employing it for checkpoint and layer selection on a DINOv2 ViT-B/14 model with registers and a randomly initialized classifier [42].

Checkpoint selection. We fully finetune a DINOv2 model for 150 epochs and compare checkpoints selected by different methods: our gF1 score, the arithmetic mean of accuracies on the ID training and retrieved data, accuracy on the retrieved data and ID training data only, and no selection (i.e., using the final checkpoint). As shown in Fig. 12, our gF1 score selects a checkpoint that generalizes effectively to both ID and OOD test data.

Layer selection. Table 7 reports the results of partially finetuning (PFT) the top- k layers of DINOv2. It reveals a

Table 8. **Averaged accuracy with standard deviations.** For each method, we run three times using different few-shot training data and report the average accuracy and standard deviation on ImageNet (as ID test set) and its variants (as OOD test sets). Our proposed methods demonstrate superior accuracy and stability.

	methods	venue&year	validation	ID test			OOD test			avg.
				IN	IN-V2	IN-S	IN-A	IN-R		
Prompt Tuning	CoOp [71]	IJCV'22	ID test acc.	71.74±0.16	64.57±0.22	47.54±0.31	50.40±0.25	75.58±0.36	59.52±0.28	
	MaPLe [25]	CVPR'23	ID test acc.	71.05±0.17	64.27±0.33	48.74±0.45	50.72±0.20	77.22±0.34	60.24±0.29	
	VPT _{shallow} [22]	ECCV'22	ID test acc.	72.61±0.20	65.51±0.30	49.08±0.21	49.72±0.47	78.51±0.13	60.70±0.23	
	VPT _{deep} [22]	ECCV'22	ID test acc.	72.63±0.14	65.14±0.23	47.67±0.23	47.28±0.50	76.59±0.16	59.17±0.26	
Adapter Learning	Tip-Adapter [68]	ECCV'22	ID test acc.	70.53±0.03	63.26±0.09	48.68±0.06	50.90±0.09	77.80±0.07	60.16±0.04	
	Tip-Adapter-F [68]	ECCV'22	ID test acc.	73.34±0.14	65.32±0.19	47.72±0.33	48.91±0.27	76.63±0.29	59.79±0.16	
	CLIP-Adapter [9]	IJCV'23	ID test acc.	71.48±0.14	63.88±0.15	46.49±0.20	47.65±0.58	73.78±0.36	57.95±0.25	
	TaskRes [63]	CVPR'23	ID test acc.	73.42±0.10	65.27±0.19	48.08±0.05	49.27±0.70	76.93±0.29	59.89±0.16	
	LoRA [19]	ICLR'22	ID test acc.	73.01±0.12	65.56±0.22	48.59±0.20	50.51±0.42	77.85±0.24	60.63±0.09	
Linear Probing	LP [48]	ICML'21	ID test acc.	73.54±0.20	65.48±0.24	48.78±0.25	49.59±0.21	77.65±0.45	60.37±0.16	
	LP w/ WiSE-FT [60]	CVPR'22	ID test acc.	71.93±0.04	64.66±0.22	49.44±0.01	50.62±0.07	78.33±0.03	60.76±0.04	
	CMLP [33]	CVPR'23	ID test acc.	73.38±0.07	65.14±0.30	48.52±0.33	49.10±0.48	77.42±0.17	60.05±0.11	
	LP w/ LCA [53]	ICML'24	ID test acc.	69.34±0.07	62.53±0.11	48.52±0.02	49.47±0.19	77.76±0.05	59.57±0.05	
	CLAP [54]	CVPR'24	val-free	72.86±0.13	65.06±0.06	47.79±0.19	49.58±0.22	77.09±0.24	59.88±0.08	
Finetuning	FLYP [11]	CVPR'23	ID test acc.	74.14±0.16	65.50±0.05	47.29±0.09	45.43±0.62	74.82±0.34	58.26±0.13	
	FFT [35]	CVPR'25	val-free	72.37±0.10	64.85±0.25	48.09±0.30	48.97±0.33	75.67±0.50	59.39±0.20	
	SWAT [35]	CVPR'25	val-free	73.56±0.07	66.57±0.15	54.89±0.09	50.85±0.23	81.18±0.07	63.37±0.03	
	VEST	ours	gF1 score	75.66±0.03	68.69±0.12	54.81±0.05	52.94±0.10	81.22±0.08	64.42±0.05	

clear trade-off: increasing the number of fine-tuned layers enhances ID accuracy but substantially degrades OOD performance. Our gF1 score selects the top-1 layer for PFT, achieving a favorable balance between ID and OOD performance and demonstrating its effectiveness in guiding layer selection for robust adaptation.

F. Details of Compared Methods

To evaluate the performance stability of both baselines and the proposed method, we conduct three runs with different 16-shot training data splits and compute the mean accuracy and standard deviations. Results in Table 8 demonstrate that our method exhibits low variance and hence better stability. We describe the compared methods as below, categorized into four groups.

- **Prompt Tuning** methods adapt VLM through learnable prompt tokens without adapting the whole VLM. Among them, CoOp [71] and CoCoOp [70] optimize text prompt tokens for the language branch, while VPT [22] introduces learnable prompts for visual inputs. MaPLe [25] simultaneously learns prompts for both visual and textual modalities. ProText [26] leverages large language model knowledge to learn text prompts without visual supervision.
- **Adapter Learning** methods adapt VLM by introducing lightweight trainable modules while keeping the backbone frozen. Tip-Adapter [68] implements a key-value cache mechanism derived from few-shot training examples. CLIP-Adapter [9] introduces an adapter consisting of two linear layers. TaskRes [63] learns a target task classifier by optimizing a set of task-specific residual parameters. DMN-ZS [69] proposes dual memory networks

to preserve knowledge of few-shot training data and testing data. LoRA [19] adapts the large language model by incorporating learnable low-rank matrices into model weights. Following the implementation of [64], we apply LoRA specifically to the vision encoder of VLM.

- **Linear Probing** methods adapt pretrained VLM by training a linear classifier on the frozen visual encoder. LP w/ WiSE-FT [60] employs weight-space ensembling, combining classifier weights with the pretrained model. We use an interpolation factor of 0.5 in our experiment. CMLP [33] leverages multimodal examples as additional training examples. LP w/ LCA [53] introduces WordNet class hierarchy as the soft label. CLAP [54] introduces class-adaptive penalty terms during classifier training.
- **Finetuning** methods adapt VLM by updating all parameters for downstream tasks. Standard finetuning method only finetunes the visual encoder with cross entropy loss [35], while FLYP finetunes both visual and textual encoders with contrastive loss [11]. SWAT [35] proposes a two-stage method with retrieval augmentation for few-shot learning.